Malays. J. Bioeng. Technol. Vol. 2, No. 3, (2025): 115-128
https://doi.org/10.70464/mjbet.v2i3.1710

MALAYSIAN JOURNAL OF BIOENGINEERING AND TECHNOLOGY

MJBeT Malaysian Journal of Bioengineering and Technology

Ion Exchange of Lanthanum Chloride and Lewatit MonoPlus S 108 H Resin

Norazihan Zulkifli[1], Noor Fazliani Shoparwe[1,*], Abdul Hafidz Yusoff[1], Ahmad Zuhairi Abdullah[2], Mohammad Norazmi Ahmad[3]

[1]*Gold Rare Earth and Material Technopreneurship Centre (GREAT), Faculty of Bioengineering and Technology, Universiti Malaysia Kelantan, 17600 Jeli, Kelantan, Malaysia*
[2]*School of Chemical Engineering, Engineering Campus, Universiti Sains Malaysia, 14300 Nibong Tebal, Pulau Pinang, Malaysia*
[3]*Sustainable Nanotechnology and Computational Chemistry (SuNCoM) Research Group, Department of Chemistry, Kulliyyah of Science, International Islamic University Malaysia, 25200 Kuantan, Pahang, Malaysia*

**Corresponding author: fazliani.s@umk.edu.my*

ARTICLE INFO

Received:1 September 2025
Accepted:18 September 2025
Online:30 September 2025
eISSN: 3036-017X

ABSTRACT

Rare Earth Elements (REEs) are indispensable for numerous advanced technologies; however, their supply chain faces significant challenges due to geopolitical factors and the environmental impact of conventional mining methods. This study investigates the potential of ion exchange adsorption for the recovery and separation of REEs from a novel secondary source: carbonate precipitates derived from ionic clay leachates. Specifically, the performance of Lewatit MonoPlus S 108 H, a strong acid cation exchange resin, was evaluated through comprehensive batch adsorption experiments. The research encompassed kinetic and isotherm modelling. Kinetic studies revealed that the adsorption of lanthanum in chloride media at pH 2 followed the Pseudo-Second-Order model, indicating chemisorption as the rate-limiting step. Equilibrium data were best described by the Langmuir isotherm, with a maximum adsorption capacity (Q_m) of 82.64 mg/g, suggesting monolayer adsorption on a homogeneous surface. The findings confirm the viability of Lewatit MonoPlus S 108 H for the selective recovery of rare earth elements from complex, secondary streams. This offers a sustainable pathway for the critical element supply.

Keywords: REE; Lewatit MonoPlus S 108 H; adsorption; kinetics; modelling; isotherm

1. Introduction

Rare Earth Elements (REEs), a group of 17 chemically similar metallic elements comprising 15 of lanthanides lanthanum (La), cerium (Ce), praseodymium (Pr), neodymium (Nd), samarium (Sm), europium (Eu), gadolinium (Gd), terbium (Tb), dysprosium (Dy), holmium (Ho), erbium (Er), thulium (Tm), ytterbium (Yb), and lutetium (Lu), plus scandium (Sc) and yttrium (Y) in the periodic table [1-3]. They are pivotal to modern technological advancements. Their unique magnetic, catalytic, and optical properties render them indispensable components in a vast array of high-tech applications, including electric vehicles, wind turbines, consumer electronics, medical imaging, and defence systems [4].

REEs have been primarily sourced from hard rock ore deposits such as bastnäsite, a fluorocarbonate mineral of formula (Ce, La, Y, F)CO_3, and monazite, a phosphate mineral of formula ((Ce, La, Th)PO_4) [5-7]. They are also found in ion-adsorbed clays (IAC) in sub-tropical to tropical climate regions, from weathered granite, such as southern China and Southeast Asia [8]. These REEs are typically leached from laterite clay using ammonium sulphate solution by in-situ leaching (ISL), producing a leachate rich in dissolved REEs [9]. The dissolved REEs are then precipitated, often as rare earth carbonates, to concentrate the metals and facilitate further purification and separation steps [10]. The next step of the REE value chain is the REE separation. REE separation is a complex and challenging process due to the inherent chemical similarities among the REEs [11]. This is primarily driven by the lanthanide contraction, a steady decrease in ionic radii across the series from lanthanum to lutetium, making their separation a formidable task [12-13]. This phenomenon results in subtle differences in their chemical properties, requiring a highly selective solvent extraction technique. Solvent extraction method uses hazardous organic solvents, requiring multi-stage mixer-settler systems, and complex operational procedures [14]. Alternatively, a simpler method is by ion exchange, offering a highly promising, environmentally benign, and cost-effective alternative for REE recovery from low-volume feedstocks [15].

Adsorption, particularly ion exchange, stands out as a highly promising and environmentally favourable method for REE separation and recovery [16-18]. By the ion exchange method, an insoluble matrix of resin containing exchangeable ions selectively captures REE ions from solution. Strong Acid Cation (SAC) exchange resins are particularly effective for trivalent metal ions like REEs due to their sulfonic acid functional groups, which readily exchange hydrogen ions (or other cations) for the REE ions in solution [19]. Understanding the adsorption mechanisms, kinetics, and equilibrium behaviour of REEs on specific resins is critical for designing efficient and scalable separation processes for the recovery of REEs using SAC Lewatit MonoPlus S 108 H resin originating from ionic clay in situ leaching carbonate. This study is to investigate the recovery of lanthanum, representing the REE, in the adsorption process.

2. Materials and Methods

2.1 Materials

The adsorbent used in this study was Lewatit MonoPlus S 108 H, a microporous, strong acid cation exchange resin manufactured by LANXESS, Germany. The resin consists of a polystyrene-divinylbenzene (PS-DVB) copolymer matrix with sulfonic acid functional groups. Prior to use, the resin was pre-treated by washing with deionized water, cycling, conditioning with 1 M HCl cycles, and converting to the H-form. Lanthanum oxide of high purity, 99.9%, was purchased from China and used to prepare a synthetic lanthanum chloride solution for this study. All chemicals used, including hydrochloric acid (HCl), and sodium hydroxide (NaOH), were of analytical reagent grade and purchased from Merck. Deionized water (resistivity > 18 MΩ·cm) was used for all solution preparations and dilutions.

Elemental composition was determined by Inductively Coupled Plasma - Optical Emission Spectrometry (ICP-OES). A multi-station magnetic stirrer, MH6Pro (Joan Lab Equipment, China), was used for batch adsorption experiments. Solution pH was measured using an EUTECH Instrument PC700 pH/mV/Conductivity/°C/°F calibrated with standard buffer solutions. Elemental concentrations were determined using Agilent 5100 Inductively Coupled Plasma – Optical Emission Spectrometry (ICP-OES) (Agilent Technologies, USA). Other equipment included analytical balances (precision ±0.0001 g), volumetric flasks, conical flasks, and membrane filters of 0.45 μm.

2.2 Experimental Procedures

Lanthanum was selected to represent REE for optimizing the ion exchange process on Lewatit MonoPlus S 108 H resin and subsequent rate and capacity test for kinetic and isotherm modelling. Synthetic lanthanum chloride solution was prepared by dissolving lanthanum oxide, La_2O_3, 99.9% purity, in hydrochloric acid (HCl). The reaction is as Equation 1:

$$La_2O_3 + 6HCl \Rightarrow 2LaCl_3 + 3H_2O \quad (1)$$

pH was adjusted using 0.1 M HCl or 0.1 M sodium hydroxide (NaOH) solution.

eISSN Number: 3036-017X

2.2.1 Optimization studies

Taguchi Design of Experiment (DoE) was used to systematically investigate and optimise the adsorption of lanthanum (La) onto Lewatit MonoPlus S 108 H. The objective was to obtain the optimal adsorption capacity at equilibrium (q_e, mg/g) with minimal effect of variation from uncontrollable factors.

The Taguchi method is a powerful and efficient statistical tool for optimising complex processes. It minimises the number of experimental runs compared to traditional full factorial designs while still identifying significant factors and interactions. This approach aims to make the process robust and insensitive to uncontrollable factors (noise) and find the optimal setting with minimal effect of variation on the response [20-21]. This approach is particularly beneficial for processes with multiple variables, allowing for the determination of optimal process parameters that yield high performance and consistent results [22].

In this study, a five-factor, three-level Taguchi DoE was designed using Minitab statistical software. The five key process parameters are presented in Table 1, along with their respective levels.

Table 1: Five-factor and three-level Taguchi DoE

No	Factors	Level 1	Level 2	Level 3
1	Concentration (La_2O_3 g/L)	0.5	1.0	1.5
2	Resin (g)	0.5	1.0	1.5
3	Volume (mL)	20	30	40
4	pH	1	2	3
5	RPM	200	300	400

To evaluate the influence of the five key process parameters, an L27 orthogonal array was chosen. This resulted in 27 experimental runs, which is significantly fewer than the 243 runs required for a full factorial design 3^5.

Main response adsorption capacity at equilibrium (q_e, mg/g), and the extraction percentage (%R) were calculated using the following Equations 2 and 3, respectively.

$$q_e = \frac{(C_0 - C_e)V}{W} \tag{2}$$

$$\%R = \frac{(C_0 - C_e)}{C_0} \times 100 \tag{3}$$

where c_0 is the initial REE concentration (mg/L), c_e is the equilibrium REE concentration (mg/L), V is the volume of the solution (L), and W is the mass of the adsorbent (g).

From the Taguchi DoE, twenty-seven batch experiments were planned with a unique combination of the five selected factors. Each of the experiments was conducted in 100 mL glass beakers with 60 minutes of contact time. The solutions and resins were agitated using a magnetic stirrer on an orbital shaker at a set speed. At the end of the experiments, the solutions were separated from the resin by filtration using 0.45 µm syringe filters. All experiments were performed in triplicate, and the average values were used for data analysis. The filtrate was then collected for elemental analysis by ICP-OES.

The runs generated by the L27 array allowed for the calculation of Signal-to-Noise (S/N) ratios, chosen with a 'Larger-the-better' criterion to maximize adsorption capacity, and subsequent Analysis of Variance (ANOVA) to determine the statistical significance and percentage contribution of each factor.

2.2.2 Kinetic studies

Kinetic experiments were performed under fixed optimal conditions, an initial La concentration of 10 La_2O_3 g/L, a resin dosage of 30 g, a solution volume of 500 ml, a stirring speed of 400 RPM, and at a room temperature of

eISSN Number: 3036-017X

27°C. Samples of the solution were withdrawn at predetermined time intervals (every 0.5 minutes for 5 minutes, 2 to 3 minutes over the next 15 minutes, every 5 minutes to the hour, and approximately 10 minutes to the end of the experiment time, filtered, and analysed for residual La concentration.

The experimental kinetic data were fitted to the linear forms of the Pseudo-First-Order (PFO) as in Equation 4 and the Pseudo-Second-Order (PSO) model Equation 5:

$$\ln(Q_e - Q_t) = \ln Q_e - k_1 t \tag{4}$$

where k_1 is the PFO rate constant (min^{-1}).

$$\frac{t}{Q_t} = \frac{1}{k_2 Q_e^2} + \frac{t}{Q_e} \tag{5}$$

where k_2 is the PSO rate constant (g/mg·min).

The model parameters and correlation coefficients (R^2) were determined from the linear plots.

2.2.3 Isotherm studies

Isotherm experiments were conducted by varying the initial La concentration from 1 to 8 La_2O_3 g/L, while keeping other parameters constant: resin dosage of 0.3 g, solution volume of 30 mL, stirring speed of 400 RPM, and at a room temperature of 27°C. The contact time was set to 1 hour, which was determined from kinetic studies to be sufficient for reaching equilibrium. After equilibrium, solutions were filtered and analysed. Equilibrium concentrations (C_e) were determined by analysing the final solution, and adsorption capacities (Q_e) were calculated using the mass balance equation.

The equilibrium adsorption data were analysed using the linear forms of Langmuir, Freundlich, Temkin, and Dubinin-Radushkevich (D-R) isotherm models as Equations 6, 7, 8, and 9:

$$\frac{C_e}{Q_e} = \frac{1}{K_L Q_m} + \frac{C_e}{Q_m} \tag{6}$$

where Q_m is the maximum monolayer adsorption capacity (mg/g) and K_L is the Langmuir constant (L/mg). The dimensionless separation factor (R_L) was calculated as R_L=1/(1+).

$$\ln Q_e = \ln K_F - \frac{1}{n} \ln C_e \tag{7}$$

where K_F is the Freundlich constant ((mg/g)(L/mg)$^{1/n}$) and n is the adsorption intensity.

$$Q_e = \frac{RT}{b_T} \ln A_T + \frac{RT}{b_T} \ln C_e \tag{8}$$

where R is the ideal gas constant (8.314 J/mol·K), T is the absolute temperature (K), b_T is the Temkin constant (J/mol), and A_T is the Temkin binding constant (L/mg).

$$\ln Q_e = \ln Q_m - K_{DR} \epsilon^2 \tag{9}$$

where Q_m is the theoretical maximum adsorption capacity (mg/g), K_{DR} is the D-R constant (mol^2/J^2), and ϵ is the Polanyi adsorption potential, $\epsilon = RT \ln(1+1/C_e)$. The mean free energy of adsorption Є was calculated as E=1/ .

For models involving logarithmic transformations (Freundlich, Temkin, D-R), data points with C_e of zero were excluded from the linear regression to avoid mathematical singularities.

eISSN Number: 3036-017X

3. Results and Discussion

3.1 Optimization by Taguchi Method

The 27 experimental runs, designed through the Taguchi L27 orthogonal array, are presented in Table 2. Each experiment represents a unique combination of the five selected factors, initial La concentration ("Conc"), resin weight (Resin), solution volume (Volume), pH, and stirring rate (RPM), and the three levels. Included also are their corresponding calculated, liquid-solid ratio (L/S), La recovery (%R), and the resin adsorption capacity, q_e, (La^{3+}/Resin, mg/g) for each run.

Table 2: La chloride x S108H optimization – Taguchi L27 orthogonal array

No	Conc (La_2O_3 g/L)	Resin (g)	Volume (mL)	pH	RPM	L/S	%R	La^{3+}/Resin (mg/g)
1	0.5	0.5	20	1	200	10	97%	10.04
2	0.5	0.5	20	1	300	10	97%	10.06
3	0.5	0.5	20	1	400	10	97%	9.98
4	0.5	1	30	2	200	30	100%	8.34
5	0.5	1	30	2	300	30	100%	8.37
6	0.5	1	30	2	400	30	100%	8.35
7	0.5	1.5	40	3	200	27	100%	7.16
8	0.5	1.5	40	3	300	27	100%	7.16
9	0.5	1.5	40	3	400	27	99%	7.13
10	1	0.5	30	3	300	15	100%	29.58
11	1	0.5	30	3	400	15	100%	29.59
12	1	0.5	30	3	200	15	100%	29.64
13	1	1	40	1	300	40	97%	17.77
14	1	1	40	1	400	40	98%	18.03
15	1	1	40	1	200	40	97%	17.79
16	1	1.5	20	2	300	13	100%	6.03
17	1	1.5	20	2	400	13	100%	6.03
18	1	1.5	20	2	200	13	100%	6.03
19	1.5	0.5	40	2	400	20	100%	59.01
20	1.5	0.5	40	2	200	20	100%	59.12
21	1.5	0.5	40	2	300	20	100%	59.12
22	1.5	1	20	3	400	20	100%	17.10
23	1.5	1	20	3	200	20	100%	17.10
24	1.5	1	20	3	300	20	100%	17.10
25	1.5	1.5	30	1	400	20	97%	15.18
26	1.5	1.5	30	1	200	20	97%	15.11
27	1.5	1.5	30	1	300	20	97%	15.11

The highest adsorption capacity achieved was 59 mg/g (with the initial concentration of 1.5 La_2O_3 g/L, resin weight of 0.5g, volume of 40 mL, and pH of 2. This achievement matches reported REE adsorption on Dowex 50WX8 (a crosslinked strong cation PS-DBV resin) in the range of 10 to 60 mg/g [19,23].

eISSN Number: 3036-017X

3.1.1 Mean response analysis

Table 3 presents the mean responses for each factor and level, and Fig. 1 presents the main effect plot of response for each factor level.

Table 3: La chloride x S108H - response table for means

Level	Concentration	Resin	Volume	pH	RPM
1	8.511	32.905	11.051	14.341	18.926
2	17.832	14.438	17.697	24.488	18.923
3	30.438	9.438	28.033	17.952	18.932
Delta	21.927	23.467	16.981	10.147	0.010
Rank	2	1	3	4	5

The response for the means presented in Table 3 shows that Resin has the highest ranking, meaning it yields the highest performance. Ranking number 2 is ”Conc”, followed by Resin. The best pH was at 2, exceeding the performance at pH 1 and 4. Fig. 1 illustrates the response means graphically with respect to “Conc”, Resin, Volume, pH, and RPM. “Conc” and Volume have an increasing effect on Stirring. “RPM” does not seem to have any effect on the response at all.

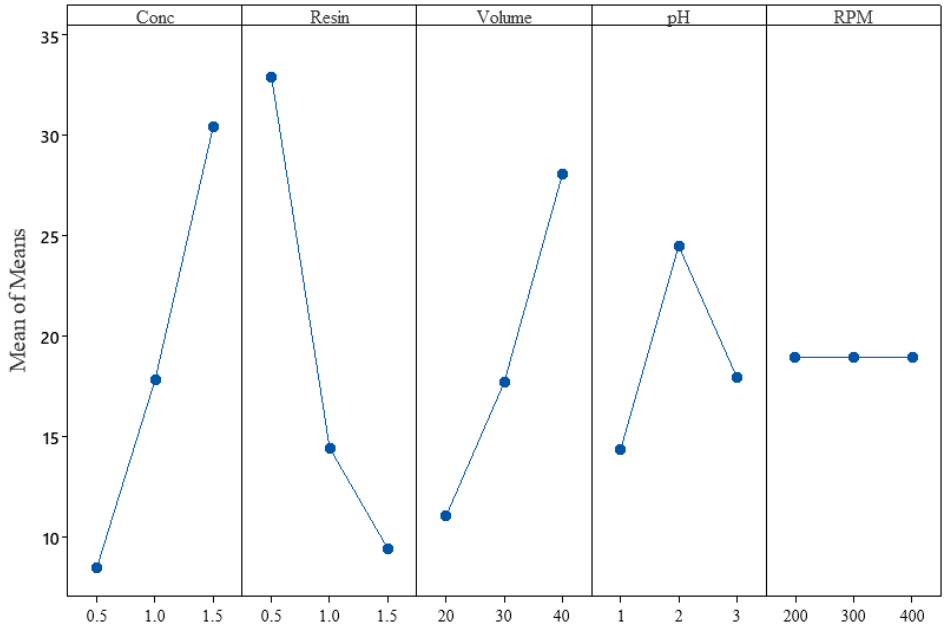

Fig. 1: La chloride x S108H – main effect plot for response (mg/g)

Therefore, based solely on the main effect plots, the optimal combination of factors for the highest lanthanum adsorption was concentration of 1.5 g La_2O_3/L, resin weight of 0.5 g, volume of 40 mL, pH of 2, stirring speed between 200 and 400 rpm, with q_e achieved at 32.9 mg/g.

3.1.2 Signal-to-Noise (S/N) ratio analysis

This section discusses the signal-to-noise ratio analysis. Table 4 presents the responses for the S/N ratio with “Larger is better”.

Table 4: La chloride x S108H – response for S/N ratios “Larger is better”

Level	Conc	Resin	Volume	pH	RPM
1	18.52	28.29	20.10	22.89	23.25
2	23.26	22.71	23.82	23.16	23.26
3	27.90	18.76	25.85	23.72	23.26
Delta	9.38	9.53	5.76	0.84	0.010
Rank	2	1	3	4	5

eISSN Number: 3036-017X

The response for S/N ratio with “Larger is better” standard deviation ranking indicates the factor with the most variation to affect the response was “Resin”, followed by “Conc”, “Volume”, “pH”, and “RPM”. The ranking indicates the resin weight has the highest variability to the response, with the largest delta at 9.53. The stirring rate has the lowest variability in the response, with a small delta at 0.010. Fig. 2 presents graphs of the S/N ratio for each factor level.

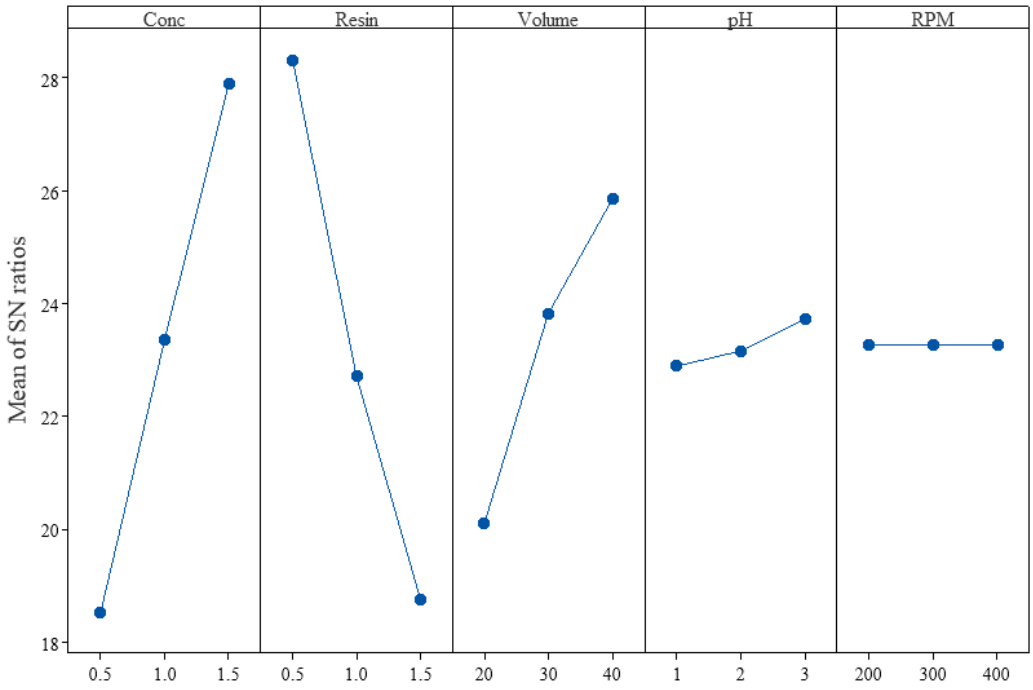

Fig. 2: La chloride x S108H - main effect plot for S/N ratios

From Fig. 2, the highest S/N ratio for “Conc” is observed at the 1.5 level of concentration. This suggests that the adsorption process is most robust (less sensitive to noise factors) when operated at this higher initial lanthanum concentration. The optimal level with the highest S/N ratio for “Resin” was 0.5 g. The response dropped sharply with an increase in resin of 1.0 and 1.5 g. This indicates that a smaller amount of Lewatit MonoPlus S 108 H resin is most effective in providing consistent and high adsorption performance, suggesting efficient utilization of active sites even at lower dosages, which can have significant economic benefits (reduced material cost) without sacrificing robustness. “Volume” of 20 ml of level 1 results in the response being the lowest. Increasing the volume to 30 and 40 mL sharply increases the response, with a more stable adsorption. The volume of 40 mL provides the most stable adsorption outcome. The high volume and low resin grammage relate to a high Liquid-to-Solid (L/S) ratio for a high adsorption performance. The optimal pH for robust adsorption is found at pH 1. A lower pH value generally indicates a more favourable environment for cation exchange, minimising interference from hydroxyl complexes and enhancing the resin's ability to bind with La^{3+} ions. The highest S/N ratio for stirring is observed at 200 RPM. This suggests that the lowest stirring speed provides the minimal physical stress on the resin beads and more efficient adsorption.

The magnitude of the slope in each factor's plot also indicates its relative impact on the S/N ratio. Visually, the "Concentration," "Resin," and "Volume" factors show particularly steep slopes, suggesting they have a more pronounced effect on the robustness and consistency of the adsorption process compared to "pH" and "Stirring," which exhibit less drastic changes across their levels.

Therefore, based solely on the S/N ratio analysis, the optimal combination of factors for robust lanthanum adsorption was a concentration of 1.5 g La_2O_3/L, resin weight of 0.5 g, volume of 40 mL, pH of 1, stirring speed of 200 rpm, with q_e achieved at 28.3 mg/g.

eISSN Number: 3036-017X

This set of conditions is predicted to yield the highest and most consistent lanthanum adsorption performance, minimising the influence of uncontrolled variations. Further analysis, as confirmation experiments, consideration of cost, and practical implementation would be necessary to validate and apply these findings in a real-world scenario.

3.1.3 Analysis of variance (ANOVA)

Table 5 presents the results of analysis of variance, showing degrees of freedom (DF), adjusted sum of squares (Adj. SS), adjusted mean square (Adj. MS), F-value, and p-value for each factor.

Table 5: La chloride x S108H - analysis of variance

Source	DF	Adj. SS	Adj. MS	F-Value	P-Value
Regression	5	5998.05	1199.61	34.69	0
Conc	1	2163.52	2163.52	62.56	0
Resin	1	2478.22	2478.22	71.66	0
Volume	1	1297.65	1297.65	37.52	0
pH	1	58.65	58.65	1.70	0.207
RPM	1	0	0	0	0.998

Statistical data from Table 5 clearly state that parameters “Conc”, “Resin”, and “Volume” had a statistically significant influence with p-value < 0.05. pH and the stirring speed (RPM) did not have a significant effect on the total variation. The regression equation is as Equation 10.

$$\text{mg/g} = -8.62 + 21.93 \text{ “Conc”} - 23.47 \text{ “Resin”} + 0.849 \text{ “Volume”} + 1.81 \text{ “pH”} \quad (1)$$

The R^2 was 0.8920.

3.1.4 Analysis of factor interactions

Beyond the individual effects of factors on the Signal-to-Noise (S/N) ratio, understanding the interactions between factors is crucial for optimising the lanthanum adsorption process. Interaction plots reveal whether the effect of one factor on the response is dependent on the level of another factor. Fig. 3 presents the interaction plots for all combinations of the five studied factors (Concentration, Resin, Volume, pH, and Stirring).

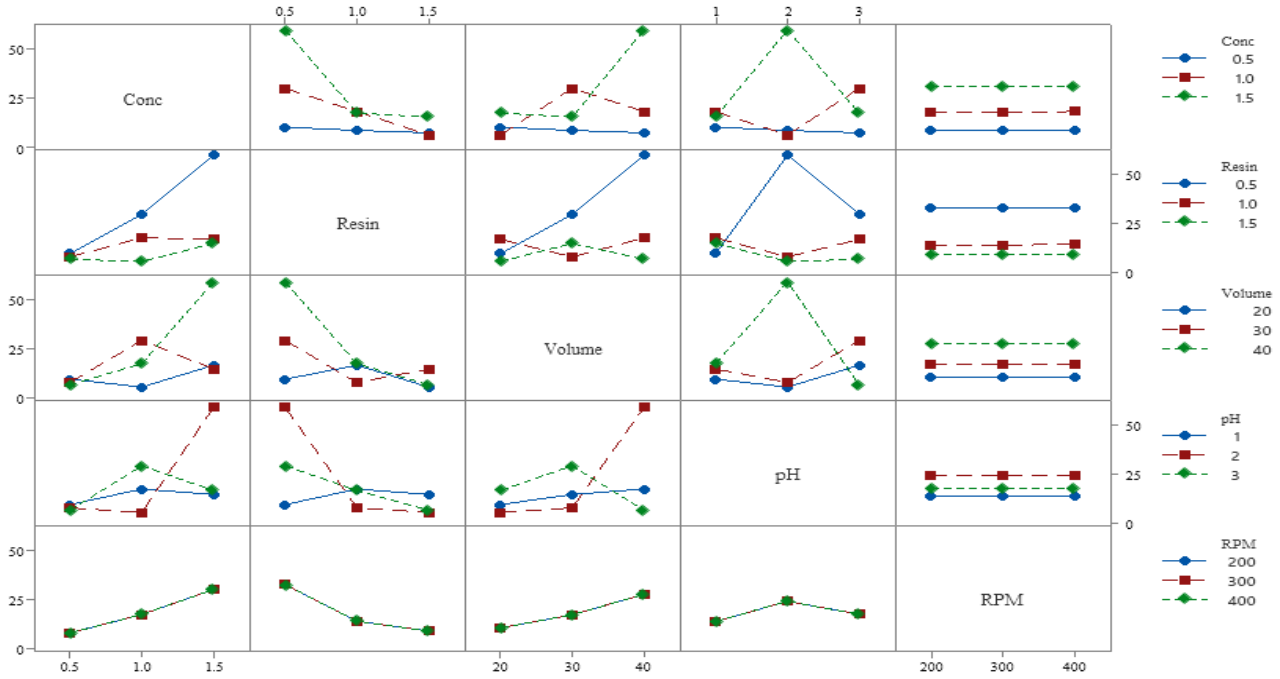

Fig. 3: La chloride x S108H – means response interaction plot for *S* (mg/g)

eISSN Number: 3036-017X

A visual inspection of Fig. 3 suggests that while some interactions are minimal (indicated by relatively parallel lines), several pairs of factors exhibit non-parallel lines, indicating the presence of significant interactions that warrant careful consideration in determining the overall optimal conditions.

“Conc” and “Resin” interaction shows noticeable non-parallel lines, particularly between the 0.5 and 1.5 g levels of Conc” across different resins. The performance of the resin appears to be dependent on the initial lanthanum concentration. The resin at a level of 0.5 g performs very well at higher concentrations. The interaction between “Conc” and “Volume” appears to be non-parallelism, suggesting that the optimal volume might depend on the initial concentration. On the other hand, the interaction between “Conc” and pH appears quite strong. The lines for different pH levels diverge significantly as concentration changes, indicating that the impact of pH on robustness is highly dependent on the initial lanthanum concentration. For example, at lower concentrations, there's less distinction, but at higher concentrations, pH 1 clearly shows superior performance. The interaction lines for “Conc” and Stirring show some divergence, suggesting an interaction where the optimal stirring speed might vary with the initial concentration.

Resin and Volume interaction lines show some crossing or significant divergence across varying volumes, implying that the optimal volume depends on the chosen resin. The interaction between “Resin” and pH appears significant, with lines crossing or diverging. The effect of pH on the S/N ratio varies depending on the resin type, indicating that certain resins perform best at specific pH levels. The interaction between resin and stirring shows some non-parallelism, indicating that the stirring speed may influence performance differently depending on the resin used.

On the other hand, the interaction between volume and pH appears significant. The optimal pH for robust adsorption is influenced by the solution volume (or L/S ratio), and vice versa. Conversely, the interaction between Volume and Stirring seems less pronounced, with lines being relatively parallel, suggesting that the stirring effect is largely independent of the volume (or L/S ratio). The interaction between pH and Stirring shows some non-parallelism, implying that the optimal stirring speed might depend on the pH of the solution.

The presence of these significant interactions means that the "optimal" settings identified from the main effects plot (where each factor's best level was chosen independently) may not represent the true global optimum. To achieve the absolute best and most robust lanthanum adsorption, it is essential to consider the synergistic effects between these interacting factors. For example, if "Conc pH" is a strong interaction, the optimal pH for a high concentration might be different from the optimal pH for a low concentration. Therefore, the final recommended optimal conditions should be chosen by identifying the specific combination of interacting factor levels that collectively maximise the S/N ratio. This often involves selecting the specific intersection point or combination of levels on the interaction plot that yields the highest response. Further analysis, such as identifying the strongest interactions and visualising the S/N ratio response surface, would provide deeper insights for precise optimisation. Table 6 summarises the interaction of the variables.

Table 6: Summary of the interaction of variables

Factor 1	Factor 2	Interaction Observed?	Description
Conc	Resin	Yes	Non-parallel, strong effect
Conc	Volume	Moderate	Some divergence
pH	RPM	Minimal	Nearly parallel lines
Resin	Volume	Yes	Noticeable interaction

3.2 Kinetics Modelling

The uptake of La onto Lewatit MonoPlus S 108 H resin was investigated over a period of 120 minutes (at fixed conditions V=500mL, m=30g, pH=1, T=room temperature). Fig. 4 (a) illustrates the decrease in pH relative to the increase in H+ reaching equilibrium about 20 minutes. Fig. 4 (b) presents the concentration changes over time, which shows the reduction of La ions during the adsorption test, reaching equilibrium within 20 minutes.

eISSN Number: 3036-017X

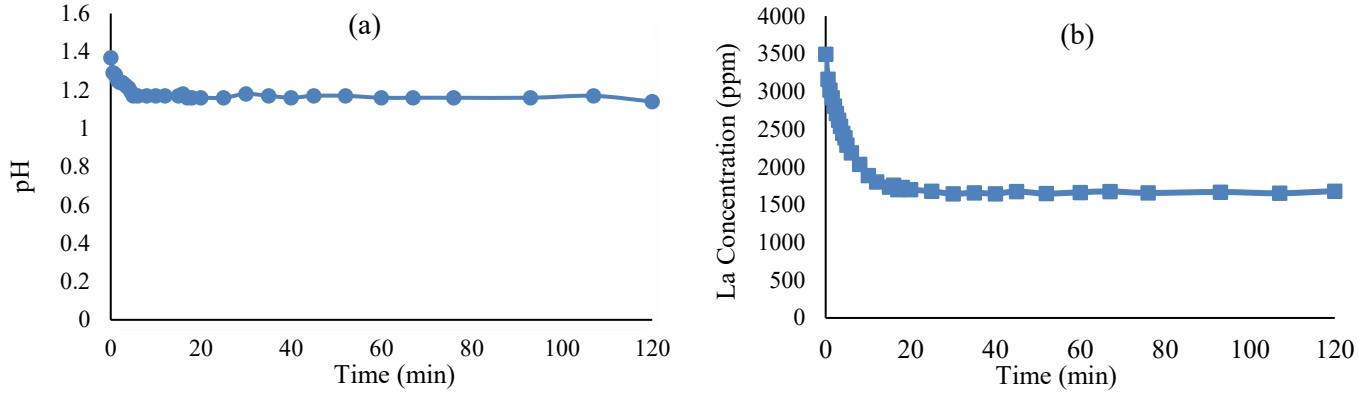

Fig. 4: La uptake on Lewatit MonoPlus S 108 H *(*a) pH*,* and *(*b) La concentration (ppm) versus time (minute)

The plots illustrate the activity of H^+ and La^{3+}, indicating ion exchange activity. The reaction is as in Equation 11.

$$3(R\text{-}SO_3^-\ H^+) + La^{3+} \rightleftharpoons (R\text{-}SO_3^-)3La^{3+} + 3H^+ \quad (2)$$

The initial rapid uptake is attributed to the abundance of available active sites on the resin surface. As these sites become saturated, the adsorption rate decreases, primarily governed by the diffusion of REE ions from the bulk solution to the active sites of the resin. To understand the adsorption mechanism, the experimental data were fitted to Pseudo-First-Order (PFO) and Pseudo-Second-Order (PSO) kinetic models. The linear plots for PFO and PSO models are presented in Fig. 5 (a) and (b), respectively.

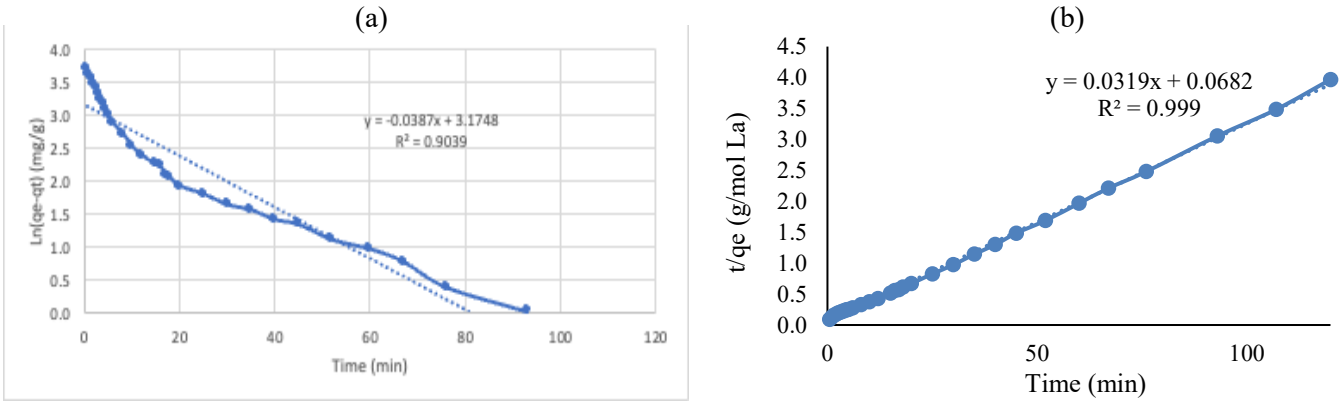

Fig. 5: (a) PFO plot, and (b) PSO plot

The kinetic parameters and correlation coefficients (R^2) are summarized in Table 7.

Table 7: Kinetic Parameters

Kinetic Model	Parameter	Value	R-squared (R^2)
PFO	k_1 (min^{-1})	0.0387	0.9039
	Q_e (mg/g)	47.06	-
PSO	k_2 (g/mg·min)	0.0046	0.9998
	Q_e (mg/g)	48.31	-

Based on the coefficient of determination (R^2), the Pseudo-Second-Order model provides a significantly better fit to experimental data (R^2=0.9998) than the Pseudo-First-Order model (R^2=0.9039). This suggests that the adsorption of La onto Lewatit MonoPlus S 108 H is predominantly governed by a chemisorption process, where the rate-limiting step involves chemical bonding between the adsorbate, La^{3+} ions, and the adsorbent, H^+ ions. The calculated equilibrium

eISSN Number: 3036-017X

adsorption capacity (Q_e) from the Pseudo-Second-Order model of 48.31 mg/g was also in good agreement with the experimental Q_e (47.06 mg/g). These findings are consistent with the works by Masry et al. [19] and Ildarabadi et al. [23] on REE adsorption on strong acid cation resins.

3.3 Isotherm Modelling

Batch uptake test across a range of initial lanthanum concentrations, from 1 to 8 g La_2O_3/L, under fixed conditions (V=30mL, w=0.3g, 1hr contact time, 400 RPM, room temp) results, including initial and final lanthanum concentrations, extraction percentage (E%), and adsorption capacity (S), are presented in Table 8.

Table 8: Resin Uptake in Varying Concentration of La^{3+} with Lewatit MonoPlus S 108 H

La_2O_3 (g/L)	$La_{initial}$ (ppm)	E (%) (Mean ± SD)	S (mg/g) (Mean ± SD)
1	530	100% ± 0%	53.31 ± 0.71
2	1006	65% ± 1%	64.67 ± 0.77
3	1454	40% ± 1%	57.92 ± 0.79
4	1834	29% ± 1%	52.98 ± 1.55
5	2184	30% ± 5%	65.29 ± 11.4
6	2468	21% ± 1%	51.13 ± 1.23
7	3023	25% ± 0%	76.01 ± 0.87
8	3625	29% ± 0%	105.94 ± 0.6

The trends observed in Table 8 are visually represented in Fig. 6 (a) for La final concentration (g/L) versus La initial concentration (g/L), (b) for E% verses La initial concentration (g/L), (c) for La Uptake (S, mg/g) versus La initial concentration (g/L), and (d) for pH changes verses La initial concentration (g/L).

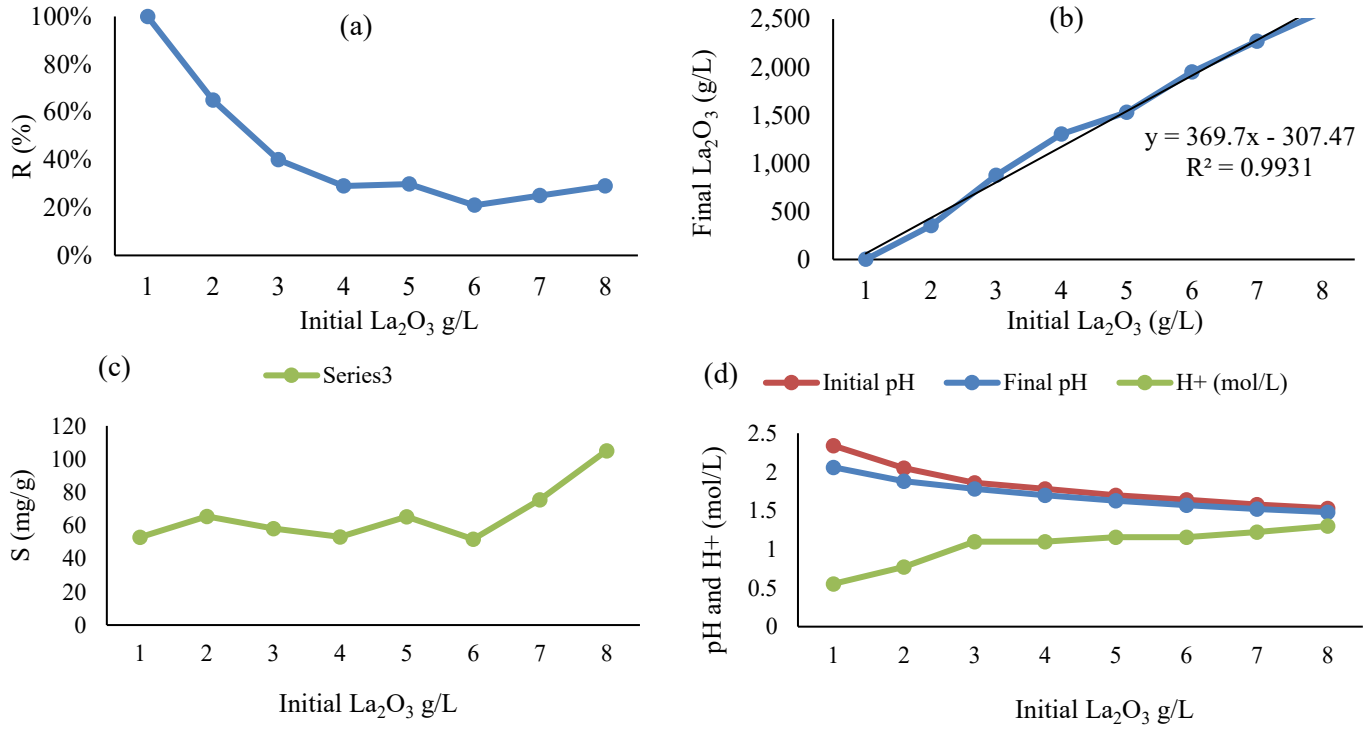

Fig. 6: Validation plots of real REE adsorption on Lewatit MonoPlus S 108 H, (a) Lanthanum Final Concentration vs. Initial La_2O_3 Concentration, (b) Lanthanum Extraction Percentage vs. Initial La_2O_3 Concentration, (c) Lanthanum Adsorption Capacity (S) vs. Initial La_2O_3 Concentration, and (d) pH and H^+ Changes for Validation Test

eISSN Number: 3036-017X

At the lowest initial lanthanum concentration (corresponding to 1 g/L La_2O_3), the resin achieved 100% extraction efficiency (E%) (Fig. 6 (a)) indicating complete removal. As the initial lanthanum concentration increased, the average extraction percentage significantly decreased, dropping to approximately 20% at the concentration of 5 g/L La_2O_3. This is expected as the fixed amount of resin becomes saturated with increasing solute load. Correspondingly, the final lanthanum concentration in solution increased linearly with initial concentration (Fig. 6 (b)).

Despite the decrease in extraction percentage, the average adsorption capacity (S mg/g) of the resin generally increased with increasing initial lanthanum concentration (Fig. 6 (c)). This demonstrates that at higher concentrations, each gram of resin is able to load more lanthanum, driven by the increased concentration gradient, until it approaches its maximum loading capacity.

Furthermore, the pH of the solution consistently decreased after adsorption (Fig. 6 (d)), indicating an increase in acidity. This is due to the release of H^+ ions from the strong acid cation exchange resin as La^{3+} ions are adsorbed, confirming the ion exchange mechanism. The magnitude of pH drop was more pronounced at lower initial lanthanum concentrations, with the H^+ concentration curve showing an initial steep increase followed by a more gradual rise, reflecting the saturation of exchange sites.

The influence of initial REE concentration on the equilibrium adsorption capacity (Q_e) was investigated, and the resulting adsorption isotherm is shown in Fig. 7. It was observed that Q_e generally increased with an increase in the initial REE concentration, indicating that a higher concentration provides a stronger driving force for the transfer of REE ions from the solution to the resin surface. At lower concentrations, the resin had abundant available sites, leading to high extraction efficiencies. As the concentration increased, the adsorption sites became progressively saturated, and the rate of increase in Q_e began to slow down, approaching a saturation point.

To further elucidate the adsorption mechanism and surface properties, the experimental equilibrium data were fitted to four widely used isotherm models: Langmuir, Freundlich, Temkin, and Dubinin-Radushkevich (D-R). The linearized plots for these models are presented in Fig. 7.

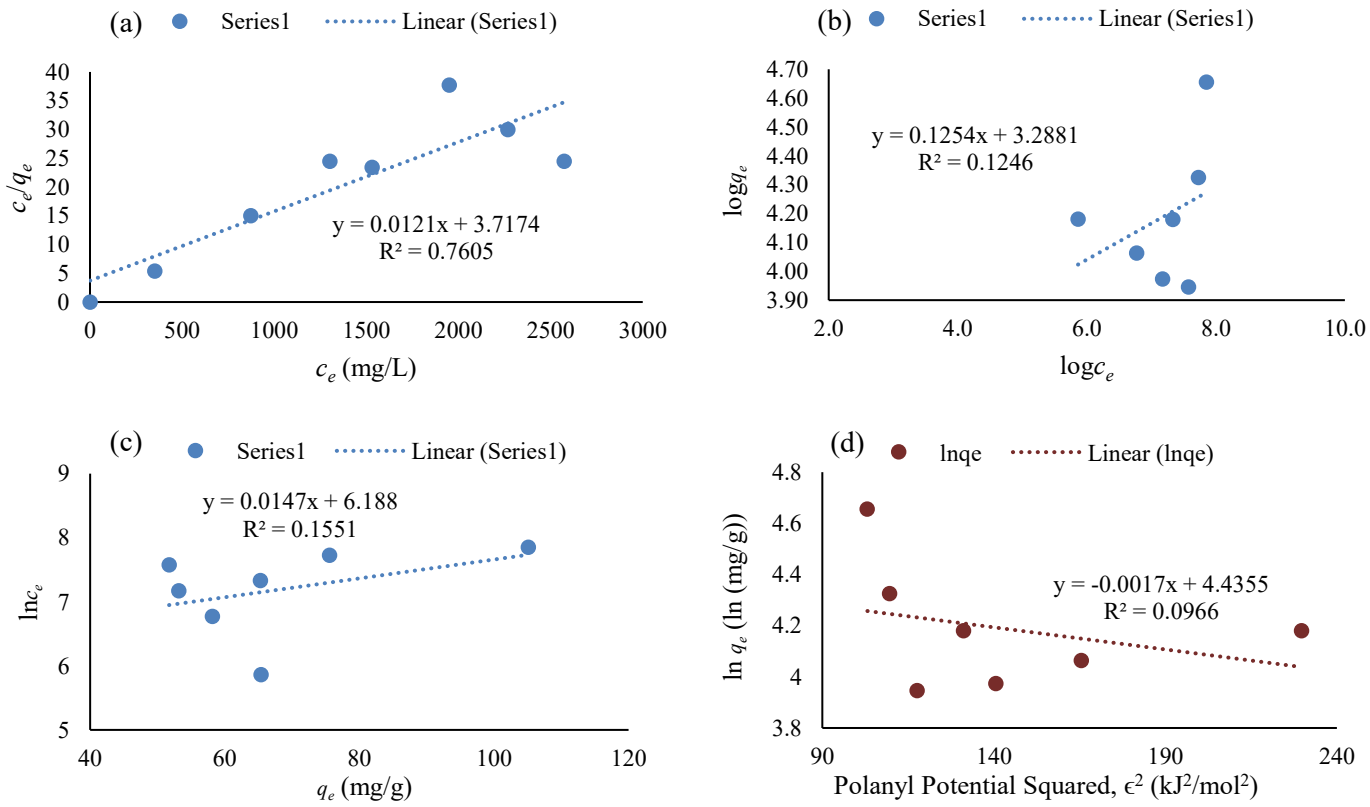

Fig. 7: Isotherm model plots for (a) Langmuir, (b) Freundlich, (c) Temkin, and (d) Dubinin-Radushkevich

eISSN Number: 3036-017X

The parameters and correlation coefficients (R^2) obtained from the linear regression analysis are summarized in Table 9.

Table 9: Number for Isotherm Parameters

Isotherm Model	Parameter	Value	R-squared (R^2)
Langmuir	Q_m (mg/g)	82.64	0.76505
	K_L (L/mg)	0.0326	-
	R_L (for max C0)	0.0781	-
Freundlich	K_F ((mg/g)(L/mg)1/n)	12.968	0.1246
	n	7.97	-
Temkin	b_T (J/mol)	236.603	0.1551
	A_T (L/mg)	0.4686	-
D-R	Q_m (mg/g)	85.51	0.0966
	K_{DR} (mol^2/J^2)	0.018	-
	E (kJ/mol)	16.67	-

Based on the R^2 values, the Langmuir isotherm model provided the best fit to the experimental data (R^2 = 0.76505), significantly outperforming the Freundlich (R^2 = 0.1246), Temkin (R^2 = 0.1551), and D-R (R^2 = 0.0966) models. This strong fit suggests that the adsorption of REEs onto Lewatit MonoPlus S 108 H primarily occurs as monolayer adsorption on a homogeneous surface with a finite number of identical active sites. The maximum monolayer adsorption capacity (Q_m) calculated from the Langmuir model was 82.64 mg/g, representing the theoretical maximum loading of REEs onto the resin. This finding is also consistent with the two other research being compared with, on REE adsorption on strong acid cation resin Dowex 50X8.

The mean free energy of adsorption (E) derived from the Dubinin-Radushkevich (D-R) model was 16.67 kJ/mol. This value falls close to the boundary range of 8-16 kJ/mol, which is characteristic of ion exchange mechanisms. This finding is consistent with the nature of Lewatit MonoPlus S 108 H as a strong acid cation exchange resin, where REE ions are adsorbed by exchanging with the hydrogen ions on the sulfonic acid groups.

4. Conclusion

This study successfully investigated the mechanism of adsorption of lanthanum using Lewatit MonoPlus S 108 H resin. Kinetic studies indicated that the adsorption process followed the Pseudo-second-order model, suggesting a chemisorption-controlled mechanism. The isotherm was best described by the Langmuir isotherm model (R^2=0.7605), confirming monolayer adsorption with a maximum capacity (Q_m) of 82.64 mg/g. The D-R model's energy value further supported an ion-exchange mechanism. This research demonstrates the viability of using Lewatit MonoPlus S 108 H resin for REE recovery from complex streams originating from ionic clays. These findings contribute to the development of more sustainable and efficient processes for securing critical REE resources. The study's limitations include batch studies not fully representing continuous column operations, a single temperature study, and a specific resin type. Future research should focus on conducting dynamic column studies to evaluate the resin's performance in continuous flow systems. This will involve investigating regeneration strategies for the loaded resin, exploring the effect of temperature on separation efficiency, and scaling up the process for pilot-plant validation. Additionally, further studies should focus on the separation of individual or groups of REEs from the complex multi-elemental solution, potentially through sequential elution or chromatographic techniques.

eISSN Number: 3036-017X

References

[1] Tian G, Xu Z, Li X, Hu Z, Zhou B. Research Progress on the Extraction and Separation of Rare-Earth Elements from Waste Phosphors. Minerals 2025;15(1):61

[2] Masmoudi-Soussi A, Hammas-Nasri I, Horchani-Naifer K, Férid M. Rare earths recovery by fractional precipitation from a sulfuric leach liquor obtained after phosphogypsum processing. Hydrometallurgy 2020;191:105253

[3] Sinha MK, Tanvar H, Sahu SK, Mishra B. A Review on Recovery of Terbium from Primary and Secondary Resources: Current State and Future Perspective. Miner Process Extr Metall Rev 2024;45(7):743–766

[4] Shetty RR, Tay BY, Goh W, Min S, Tan D, Ye S, Bu J, Huang KW, Hengne AM. Closing the Waste Loop: A Sustainable Process of Extracting Lanthanum, Mullite, Silica, and Alumina from Spent Fluidized Cracking Catalysts. Ind Eng Chem Res 2025;64(8):4250–4259

[5] McNulty T, Hazen N, Park S. Processing the ores of rare-earth elements. MRS Bull 2022;47(3):258–266

[6] Liu SL, Fan HR, Liu X, Meng J, Butcher AR, Yann L, Yang KF, Li XC. Global rare earth elements projects: New developments and supply chains. Ore Geol Rev 2023;157:105428

[7] Gaustad G, Williams E, Leader A. Rare earth metals from secondary sources: Review of potential supply from waste and byproducts. Resour Conserv Recycl 2021;167:105213

[8] Aziman ES, Ismail AF, Rahmat MA. Balancing economic growth and environmental protection: A sustainable approach to Malaysia's rare-earth industry. Resour Policy 2023;83:103753

[9] Wu Z, Chen Y, Wang Y, Xu Y, Lin Z, Liang X, Cheng H. Review of rare earth element (REE) adsorption on and desorption from clay minerals: Application to formation and mining of ion-adsorption REE deposits. Ore Geol Rev 2023;157:105446

[10] Wu M, Yu M, Cheng Q, Yuan Q, Mei G, Liang Q, Wang L. Flotation recovery of Y_2O_3 from waste phosphors using ionic liquids as collectors. Chem Phys Lett 2023;825:140608

[11] Patel DK, Sharma VK, Sharma HO. Current Global Status of Rare Earth Elements (REEs) and Their Role as Catalysts in Reducing Air Pollution for Maintaining Environmental Sustainability. Trans Indian Inst Met 2025;78(1):4

[12] Liu T, Chen J. Extraction and separation of heavy rare earth elements: A review. Sep Purif Technol 2021;276:119263

[13] Chen Z, Li Z, Chen J, Kallem P, Banat F, Qiu H. Recent advances in selective separation technologies of rare earth elements: A review. J Environ Chem Eng 2022;10(1):107104

[14] Valkov AV, Ananyeva EA, Sergievsky VV. Extraction of a target element from a mixture of rare earth elements in a single-stage process. Tsvetn Met 2022:38–43

[15] Gkika DA, Chalaris M, Kyzas GZ. Review of Methods for Obtaining Rare Earth Elements from Recycling and Their Impact on the Environment and Human Health. Processes 2024;12(6)

[16] Talan D, Huang Q. A review of environmental aspect of rare earth element extraction processes and solution purification techniques. Miner Eng 2022;179:107430

[17] Sharifian S, Wang NHL. Resin-based approaches for selective extraction and purification of rare earth elements: A comprehensive review. J Environ Chem Eng 2024:112402

[18] Sager M, Wiche O. Rare Earth Elements (REE): Origins, Dispersion, and Environmental Implications—A Comprehensive Review. Environments 2024;11(2):24

[19] Masry BA, Abu Elgoud EM, Rizk SE. Modelling and equilibrium studies on the recovery of praseodymium (III), dysprosium (III) and yttrium (III) using acidic cation exchange resin. BMC Chem 2022;16(1):37

[20] Ibrahim Idrees Ibrahim A, Aboelgamel M, Kaan Soylu K, Top S, Kursunoglu S, Altiner M. Production of high-grade antimony oxide from smelter slag via leaching and hydrolysis process. Sep Purif Technol 2025;354:129355

[21] Sonone VG, Tembhurkar. Taguchi's approach for optimization of photocatalytic process for greywater treatment and energy harvesting using ZnO/TiO_2/Ti heterojunction photoanode. Clean Technol Environ Policy 2025

[22] Nahara AR, Ningsih E, Darmawan R, Juliastuti SR. Optimization of Sidoarjo Mud Akaline Fusion Process Using Taguchi Method. Diffus Found Mater Appl 2024;37:61–68

[23] Ildarabadi A, Khajenoori M, Zahakifar F, Ghadiri A. The study of cerium separation from aqueous solutions using Dowex 50WX8 resin via ion exchange in batch and continuous mode. Sci Rep 2025;15(1):26586

eISSN Number: 3036-017X